alter the flow characteristics appreciably. Using the criterion given by Mirels,[1] it was established that the boundary-layer flow remained laminar throughout the measurements reported here. Analysis of the responses of a series of platinum film transducers, mounted flush with and along the length of the flow channel,[3] indicated shock heated gas lengths some 40-60% smaller than those predicted for fully developed flows.[5] In neon, for example, measured shock heated-gas lengths varied between 60 and 20 cm for Mach 2 and Mach 6 shock waves, respectively, and a downstream pressure of 4 Torr. The corresponding values for krypton at the same downstream pressure were 175 and 75 cm, respectively. The length of the shock heated gas was found to scale approximately linearly with pressure as expected.[3]

To map out particle trajectories in the shock heated gas, the approach of injecting a slice of ionization through the shock front and following its subsequent motion was used.[3] This involved creating a 4-6 cm long region of ionization (in the low-pressure test gas) ahead of an advancing (and itself nonionizing) shock wave. A pulse of RF power, of duration between 500 and 1500 μs, applied to a series of electrodes positioned on the outside circumference of the flow channel was used for this purpose.[4] The electrode station was positioned some 3 m downstream of the diaphragm, and the breakdown pulse was terminated prior to the arrival of the shock front at that location. The section of weakly ionized plasma (density $\sim 10^{10}/\text{cm}^3$) was swept into the shock heated gas and was transported further downstream and past a series of electrostatic-double probes mounted across the shock tube diameter.[3] A total of 10 probes at an interprobe spacing of 10 cm was used and the first probe was located at approximately 3.5 m from the diaphragm. For a known ion species the current monitored by the electrostatic probe circuitry could be related to the ion density. However, the actual ion composition in the plasma slice varied depending upon the gas being studied. For example, in studies involving the pure rare gases the dominant ion was expected to be the dimer ion of the parent rare gas[4] while in gas mixtures containing N_2, O_2, H_2O, and D_2O the dominant ions were expected to be N_2^+, O_2^+, H_3O^+, and D_3O^+, respectively. Several platinum film thermal transducers were used to define the location of the shock front. These diagnostics allowed both the shock front and plasma slice to be temporarily located to an accuracy of better than $\pm$ 5 μs.[4]

Results

An *X-T* diagram allows a convenient comparison between measured and predicted particle paths and several are collected in Fig. 1. For each plot the gas composition, Mach number and downstream pressure, P_1, is indicated and the origin defines the entry of the ionized slice into the shock-heated gas. The solid line labeled SF maps out the variation of the shock front with distance as determined from the responses of the platinum-film gages. For the range of test gas pressures and Mach numbers of interest in this study, shock attenuation was found to be less than 5%. This allowed the use of Eq.(2) to calculate trajectories in the shock heated gas.[2] By taking the maximum of the double-probe signal to correspond to the center of the plasma slice the data points (open circles) were obtained. For the experimental arrangement used, the plasma slice was found to have penetrated to approximately 30 and 70% of the available separation between the shock front and contact surface at the first and last probe station, respectively.

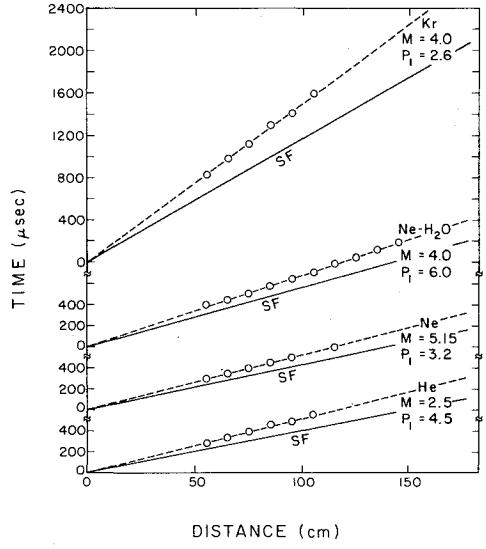

Fig. 1 Particle paths in the shock heated gas (circles represent experimental points).

The dashed line shown in Fig. 1 represents the particle paths predicted using Eq. (2). Similar agreement between measured and predicted paths was obtained for the other rare gases (argon and xenon) and for gas mixtures containing N_2 and O_2.

Summary

It appears that, at least within the limits of experimental accuracy of this study, nonuniformities associated with boundary-layer growth in developing (and nonattenuating) flow regimes can also be described using the theoretical framework presented by Mirels.[2] In situations where this test of comparing measured-particle paths with predicted-particle trajectories can be applied, the need for complex numerical analysis of flow conditions can be circumvented.

Acknowledgments

Support for this work, which was provided by the University of Texas Organized Research Funds and by the Natural Science and Engineering Council of Canada, is gratefully acknowledged.

References

[1] Mirels, H., "Flow Nonuniformity in Shock Tubes Operating at Maximum Test Times," *The Physics of Fluids,* Vol. 9, Oct. 1966, pp. 1907-1912.

[2] Mirels, H., "Boundary Layer Growth Effects in Shock Tubes," *Proceedings of the 8th International Shock Tube Symposium,* edited by J. L. Stollery, A. G. Gaydon and P.R. Owens, Chapman and Hall, London, 1971, pp. 6/1-6/30.

[3] Fox, J.N., McLaren, T.I., and Hobson, R.M., "Test Time and Particle Paths in Low-Pressure Shock Tubes," *The Physics of Fluids,* Vol. 9, Dec. 1966, pp. 2345-2350.

[4] Cunningham, A. J. and Hobson, R. M., "Dissociative Recombination at Elevated Temperatures I. Experimental Measurements in Krypton Afterglows," *Journal of Physics B, Atomic and Molecular Physics,* Vol. 5, Sept. 1972, pp. 1773-1783.

[5] Roshko, A., "On Flow Duration in Low-Pressure Shock Tubes," *The Physics of Fluids,* Vol. 3, Nov.-Dec., 1960, pp. 835-842.

AIAA 81-4113

Wing-Body Carryover at Supersonic Speeds with Finite Afterbodies

S. R. Vukelich* and J. E. Williams Jr.†
McDonnell Douglas Corporation, St. Louis, Mo.

Nomenclature

A = wing alone aspect ratio
C_{L_α} = lift curve slope for wing alone, per radian

Received Sept. 16, 1980.

*Senior Engineer-Aerodynamic Technology. Member AIAA.
†Lead Engineer-Aerodynamic Technology. Member AIAA.

C_r = wing exposed root chord
d = body diameter at wing
$K_{B(W)}$ = lift carry-over factor of body in presence of wing
M_∞ = freestream Mach number
m = cotangent of leading-edge sweep angle
r = body radius at wing
S = wing maximum semispan
S_W = wing reference area
ΔX = length of afterbody aft of wing exposed root chord trailing edge
α = angle of attack
β = Mach similarity factor, $\sqrt{M_\infty^2 - 1}$
ξ = longitudinal axis for integration
η = lateral axis for integration
λ = wing taper ratio

I. Introduction

THEORETICAL analysis of circular/cylindrical bodies with wing and/or tail combinations rely upon the aerodynamic methods developed by Pitts et al.[1] Their work developed the wing-on-body and body-on-wing carry-over factors at subsonic and supersonic speeds for linear lift. Many missile configurations today either have tail fins that have their trailing edge located at the body base or have short afterbodies. At subsonic speeds, the length of the afterbody has little significance in evaluation of wing-body carryover; at supersonic speeds it becomes important. This work expands the supersonic carry-over results of Pitts et al. to include finite afterbodies.

II. Method Description

The method used for finite afterbodies follows that of Pitts et al., which is included for completeness. Slender-body theory assumes that the additional body loading due to the presence of a wing carries straight across the body (planar model) instead of following a helix around the body (non-planar model). This planar model, though simplified, provides for simpler determination of the "lift catching area" of the body. The pressure field due to a lifting panel,[2] using the coordinate system of Fig. 1, for a panel with a supersonic leading edge is

$$P = \frac{2\alpha m}{\pi(m^2\beta^2 - 1)^{1/2}} \cos^{-1}\left(\frac{\xi/\beta + m\beta\eta}{\eta + m\xi}\right) \tag{1}$$

and for a subsonic leading edge is

$$P = \frac{4\alpha(\beta m)^{3/2}}{\pi\beta(m\beta + 1)} \left(\frac{\xi/\beta - \eta}{m\xi + \eta}\right)^{1/2} \tag{2}$$

These pressure fields were developed by assuming that the Mach wave from the wing tip leading edge is aft of the trailing edge of the wing exposed root chord, i.e., this Mach line does not cross the lift catching area of the body. Mathematically, this condition is

$$\beta A(1 + \lambda)[1 + (1/m\beta)] \geq 4 \tag{3}$$

The value of the lift transmitted to an infinite body by a wing panel is the integral of the pressure field over the lift catching area, or

$$K_{B(W)} = \frac{2L_{B(W)}}{L_W} = \frac{2}{C_{L_\alpha}\alpha S_W} \int_0^d \int_{\beta\eta}^{C_r + \beta\eta} P \, d\xi \, d\eta \tag{4}$$

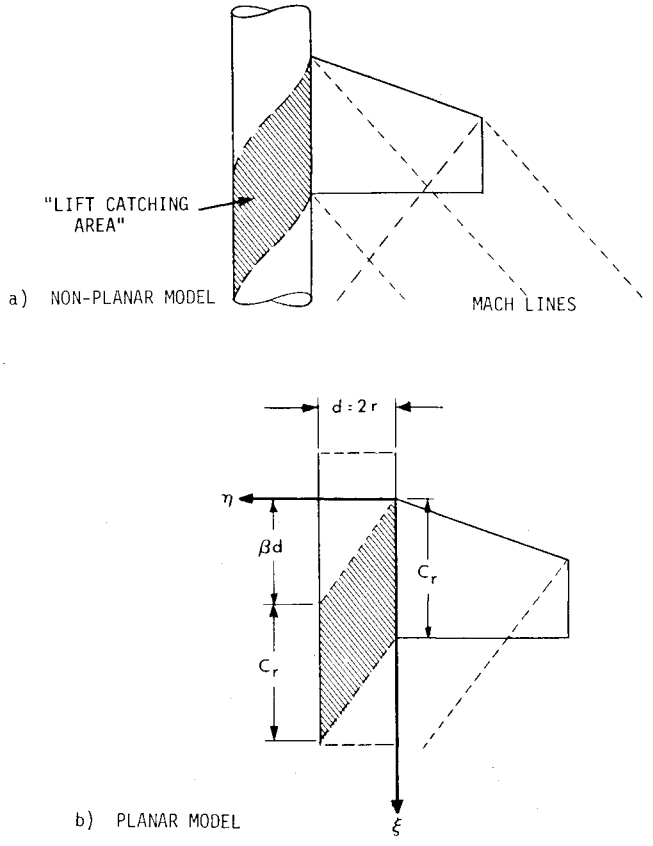

Fig. 1 Carry-over models.

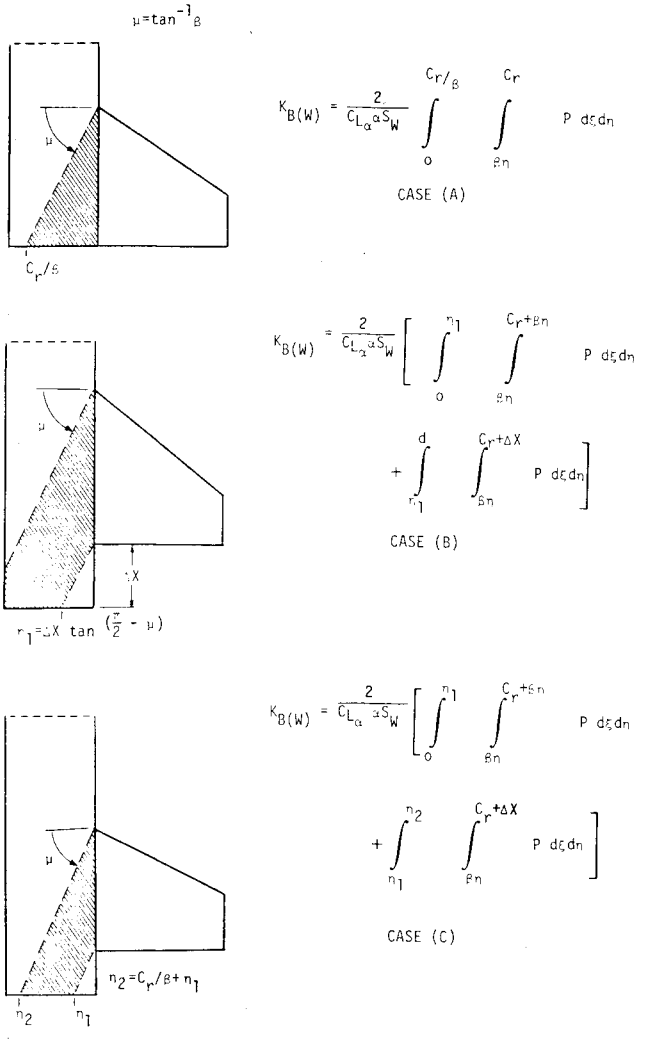

Fig. 2 Integration limits for general afterbody geometries.

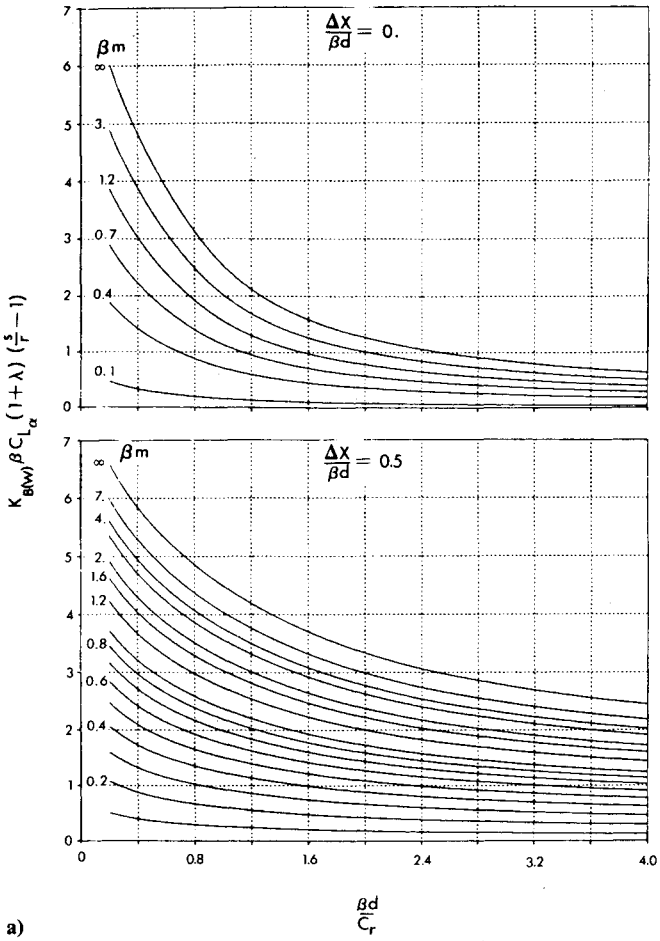

a)

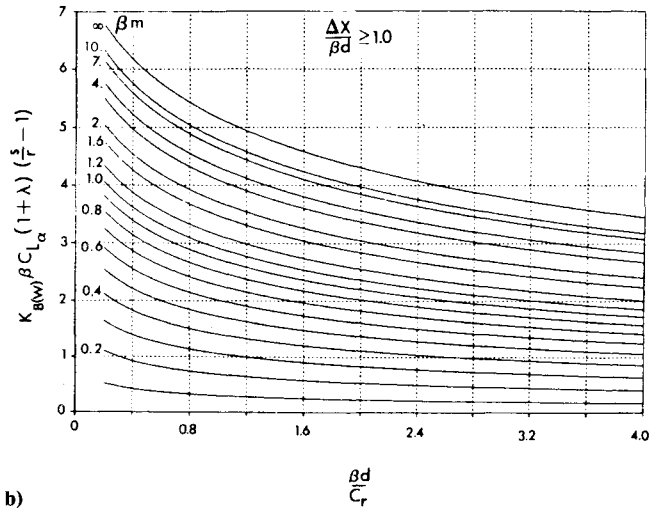

b)

Fig. 3 Body a) in presence of wing carryover for no and partial afterbodies, b) in presence of wing carryover for full afterbody.

For supersonic leading edges, this becomes (doubling for two panels)

$$K_{B(W)} = \frac{8m}{\pi(m^2\beta^2-1)^{1/2}C_{L_\alpha}S_W}\int_0^d\int_{\beta\eta}^{C_r+\beta\eta} \times\cos^{-1}\left(\frac{\xi/\beta+m\beta\eta}{\eta+m\xi}\right)d\xi d\eta \tag{5}$$

Since the wing area is

$$S_W = (S/r-1)(1+\lambda)(C_r d/2) \tag{6}$$

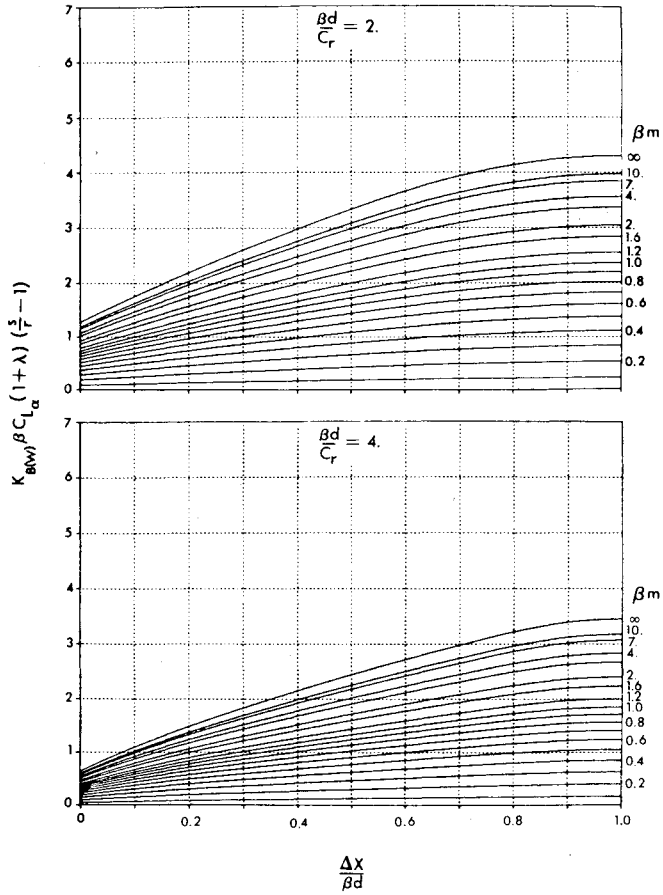

Fig. 4 Representative variation of body in presence of wing carryover as a function of afterbody length.

the equation finally reduces to

$$K_{B(W)} = \frac{8m}{\pi(m^2\beta^2-1)^{1/2}C_{L_\alpha}(S/r-1)(1+\lambda)(C_r d/2)} \times\int_0^d\int_{\beta\eta}^{C_r+\beta\eta}\cos^{-1}\left(\frac{\xi/\beta+m\beta\eta}{\eta+m\xi}\right)d\xi d\eta \tag{7}$$

A closed-form solution to this integral equation was reported by Pitts et al.

Using the same technique, the subsonic leading-edge condition results in

$$K_{B(W)} = \frac{16(\beta m)^{3/2}}{\pi\beta(m\beta+1)C_{L_\alpha}(S/r-1)(1+\lambda)(C_r d/2)} \times\int_0^d\int_{\beta\eta}^{C_r+\beta\eta}\left(\frac{\xi/\beta-\eta}{m\xi+\eta}\right)^{1/2}d\xi d\eta \tag{8}$$

which has an available closed-form solution.

The no-afterbody case is solved by letting the integration limits of ξ vary from $\beta\eta$ to C_r in the preceding integrals. When a finite afterbody is introduced, the integrals get difficult to handle by hand computation, so numerical integration of the equations is used.

The limits of integration must be changed to match the physical problem. Figure 2 shows three afterbody geometries and their corresponding limits of integration which were applied to the numerical solution of the double integrals. These limits of integration are redefined since the values of P become imaginary outside the lift catching area. A mathematical difficulty also arises at the point where $\xi=\eta=0$ (the leading edge of the root chord); the pressure formulas

become undefined, but by setting $\eta = 0$ the pressure P becomes $\cos^{-1}(1/m\beta)$ for supersonic leading edges and $\sqrt{1/m\beta}$ for subsonic leading edges and is not a function of ξ.

This method was programmed in the FORTRAN IV language and the results obtained on a CYBER 175 computer. Since computer time varies as the size of the pressure mesh defined, it became more cost effective to trade accuracy of the results with the number of mesh points. A mesh size of 50 intervals in η and 50 intervals in ξ was found to provide sufficient accuracy for engineering purposes.

III. Results of the Method

In order to provide results useful for a large variety of configurations, the results were normalized in the same manner as was done by Pitts et al. Typical results are shown in Figs. 3 and 4. Afterbody length is presented as the fraction $\Delta X/(\beta d)$, where $\Delta X/(\beta/d) = 0$ is the no afterbody case and $\Delta X/(\beta d) = 1$ is the infinite, or full, afterbody case. The results are identical to the previously published results. For some afterbody lengths an increase in carry-over lift of up to 20% over that obtained from linear interpolation between the no-afterbody and full-afterbody cases is realized.

IV. Method Extension

Since the afterbody length is arbitrary, there seems to be no difficulty in integrating the pressure field for those bodies whose base is forward of the trailing edge of the exposed root chord, for example a wing cantilevered off of the body trailing edge. These integrations have been performed and may prove useful to some specialized configurations. The limit of the method is when $\Delta X = -C_r$.

V. Conclusion

A method has been presented which evaluates the additional lift on a cylindrical body due to a lifting surface, which accounts for the effect of finite afterbodies. Extension of the method to cantilevered surfaces is also possible. Use of the method is limited within the constraints of slender-body theory and the assumptions inherent in the formulation of Pitts et al.

References

[1] Pitts, W. C., Nielsen, J. N., and Kaattari, G. E., "Lift and Center of Pressure of Wing-Body-Tail Combinations at Subsonic, Transonic, and Supersonic Speeds," NACA 1307, 1957.

[2] Nielsen, J. N., *Missile Aerodynamics*, McGraw-Hill, New York, 1960.

AIAA 81-4114

Column Creep Buckling with End Restraint

Robert L. Carlson*
Georgia Institute of Technology, Atlanta, Ga.
and
Andrew G. Morgan Jr.†
Delta Airlines, Atlanta, Ga.

Introduction

THE problem of time-dependent buckling due to creep was first recognized in 1946 by Ross.[1] The main features of results of subsequent studies are summarized in a survey article by Hoff[2] and in a book by Hult.[3] In these studies the model analyzed is a column with hinged ends, and a variety of constitutive laws are used. For a linear-viscoelastic material column, deflection tends to infinity as time goes to infinity. If either a nonlinear time-dependent or nonlinear time-independent component of strain is present, a finite critical time is observed, and the load capacity of the column tends to zero with increasing deflection.

Recently, Huang[4] observed that the small deflection limitation used in previous analyses is not consistent with the fact that very large deflections develop as the critical time is approached. By performing a large deflection analysis, Huang[4] showed that finite critical times occur only if a lower bound load is exceeded. The nonlinear properties of constitutive laws lead to softening effects which produce the feature of finite critical time. Huang introduces geometrical nonlinearities that produce a stiffening effect which can effectively result in either longer critical times or no finite critical time.

Structural systems usually consist of many elements, and they are not free to move independently. The interactions between members are restraints of a geometric character which can further modify behavior. One form of restraint is illustrated by the column shown in Fig. 1. Clearly, the axial restraint introduced by the spring will cause a redistribution of the applied load. As the column-end displacement increases, the force in the spring increases and the force acting on the column decreases. The objective of this Note is to describe the features of this redistribution process.

Analysis

The column shown in Fig. 1 has an initial imperfection of $\bar{v}_0$, which is a function of position $\bar{x}$. The column has a two flange cross-section with each flange having an area of $A/2$ and a flange separation of h. The end restraint is represented here by a linear elastic spring.

The constitutive equations for the flanges are

$$\dot{\epsilon}_c = \frac{\dot{\sigma}_c}{E} + \left(\frac{\sigma_c}{B}\right)^m \tag{1}$$

$$\dot{\epsilon}_t = \frac{\dot{\sigma}_t}{E} + \left(\frac{\sigma_t}{B}\right)^m \tag{2}$$

where ϵ and σ are strain and stress, respectively, and the dot indicates differentiation with respect to time. The subscripts c and t refer to the concave and convex flanges. Young's modulus is E, and B and m are constants for the creep-strain rate component.

The flange stresses can be computed in terms of the nondimensional deflection $v = 2\bar{v}/h$ as

$$\sigma_c = -P/A(1+v+v_0) \tag{3}$$

$$\sigma_t = -P/A(1-v-v_0) \tag{4}$$

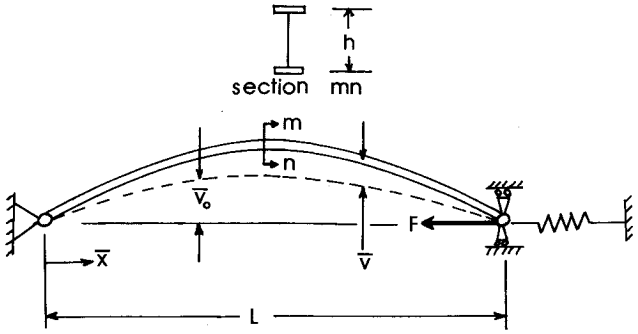

Fig. 1 Column model.

Received Sept. 4, 1980; revision received Nov. 17, 1980.

*Professor, School of Aerospace Engineering. Associate Fellow AIAA.

†Aircraft Performance Engineer, Engineering Department. Member AIAA.